CrossMark

*J. Fluid Mech.* (2020), *vol*. 903, A36. © The Author(s), 2020.
Published by Cambridge University Press
doi:10.1017/jfm.2020.656



# Trapped continental shelf waves with a free surface

**G. Kaoullas**[1],† **and E. R. Johnson**[2]

[1]Department of Mathematics and Statistics, University of Cyprus, Nicosia, Cyprus

[2]Department of Mathematics, University College London, London WC1H 0AY, UK

(Received 10 December 2019; revised 14 May 2020; accepted 30 July 2020)

A number of recent results have shown that within the shallow water, rigid-lid approximation, alongshore variations in the bathymetry, i.e. a submerged ridge, can lead to continental shelf waves (CSWs) that are localised geographically at the ridge and then decay both along and away from the coast. Removing the rigid-lid assumption, introduces the superinertial Poincaré waves and a Kelvin wave that is present at all frequencies. This implies that the spectrum of the associated wave operator, which is bounded for the rigid lid case, is continuous and unbounded for the free-surface case. In the rigid-lid case the localisation of modes are isolated eigenvalues lying above the continuous spectrum whereas any localised modes for the free-surface problem must necessarily be embedded in the continuous spectrum. The purpose of this work is to construct trapped CSWs analytically and numerically for a non-rectilinear shelf. A regular asymptotic method is employed by considering a slowly varying, non-rectilinear shelf with an approximate boundary condition at the shelf–ocean boundary. It is shown that even with the free-surface present, trapped CSWs do indeed exist for the submerged ridge topography. Comparison with highly accurate numerical results demonstrates the accuracy of the asymptotic method and also allows the consideration of shelves that abut an open ocean so avoiding the approximate boundary condition at the shelf–ocean boundary.

**Key words:** shallow water flows, topographic effects

## 1. Introduction

Continental shelf waves (CSWs) account for much of the low-frequency energy measured along coastlines. Since their discovery (Robinson 1964) there has been considerable discussion about continental shelves that account for depth changes only away from the coast while the depth remains unchanged along the coast. Huthnance (1975) has shown that for such a shelf superinertial waves exist, which include edge waves and Poincaré waves, as well as subinertial waves, which include CSWs and a Kelvin wave. If the ratio of the derivative of the depth function to the depth function is bounded everywhere, then the group velocity, $c_g$, of CSWs is oppositely signed for long and short waves so that long waves travel with shallow water to the right and short

† Email address for correspondence: g.kaoullas@gmail.com

https://doi.org/10.1017/jfm.2020.656 Published online by Cambridge University Press

waves with shallow water to the left. This implies that for such depth profiles, there is an intermediate wavenumber where CSWs have a maximum frequency for propagation, i.e. a cutoff frequency, and disturbances whose frequency exceeds the cutoff frequency are evanescent. Historically these CSWs were termed 'trapped', as they are trapped against the coast, although they propagate along the coast.

Continental shelf profiles, however, may vary alongshore. Grimshaw (1977) and Huthnance (1987) discuss slow changes in the offshore wave profile and the propagation speed of CSWs as a shelf varies slowly in the alongshore direction. This implies that the $c_g$ of any particular mode, at a fixed frequency, can vary in the alongstream direction and thus can vanish at more than point. It is shown in Kaoullas & Johnson (2012) and Johnson & Kaoullas (2011), that in the rigid-lid limit sufficiently large alongshore depth changes can lead to a local increase or a decrease in the cutoff frequency for propagation of CSWs. In particular, changes in the distance of the shelf break from the coastline or the slope of the shelf can be sufficient to create a localised region where CSWs can propagate at a higher frequency compared with the far field further along the coast. This leads to the possibility of CSWs becoming trapped both away from the coast and also away from the localised alongshore depth region so no energy at this higher frequency propagates along the coast. These modes consist of a slowly varying long wave, propagating with shallow water to the right until the $c_g$ vanishes, at which point it reflects as a short wave propagating with deep water to its right, until its $c_g$ vanishes and it is reflected back as long wave. These modes are then confined along the coast and will be referred to below as trapped CSWs (tCSWs). Examples of shelf-coastline geometries that admit tCSWs (i.e. submerged ridges and bays) were shown with asymptotic and numerical methods in Kaoullas & Johnson (2012). Changes in coastline curvature (while isobaths remained parallel to the coast) have also been shown by Johnson, Levitin & Parnovski (2006) rigorously to admit tCSWs under (weak) geometric assumptions provided the shelf bends towards the coast, i.e. shallow water. Explicit examples of such curved coastline geometries where given in Postnova & Craster (2008), Kaoullas & Johnson (2010*b*) and Kaoullas & Johnson (2012).

Trapped modes exist in other physical settings. Asymptotic and numerical results have been obtained for problems concerning waveguides in elasticity (Gridin, Craster & Adamou 2005; Kaplunov, Rogerson & Tovstik 2005; Postnova & Craster 2008) and existence proofs given for quantum (Exner & Seba 1989; Duclos & Exner 1995; Dittrich & Kriz 2002; Krejčiřík & Kříž 2005) and acoustic problems (Evans, Levitin & Vassiliev 1994; Davies & Parnovski 1998; Aslanyan, Parnovski & Vassiliev 2000). The acoustic waveguide problem (with Neumann boundary conditions) corresponds directly to non-rotating water waves in an infinitely long channel of constant depth. These problems are of particular interest as the essential spectrum of the frequency is bounded at zero, i.e. $[0, \infty)$, but the addition of symmetric, fully submerged obstacles (see e.g. Evans *et al.* 1994; Linton & McIver 1998, 2007) leads to a discrete eigenvalue lying inside the essential spectrum giving an embedded trapped mode.

Approximating the full shelf wave problem by taking the water surface to be rigid allows a stream function formulation of the problem (Buchwald & Adams 1968; LeBlond & Mysak 1978) where the Kelvin and Poincaré waves are absent and the continuous frequency spectrum has an upper bound, i.e. the cutoff frequency (Johnson *et al.* 2006). The eigenvalue problem for the frequency $\omega$ is linear and the boundary condition (b.c.) at the coast is Dirichlet. The rigid-lid approximation is valid for where the external Rossby radius of deformation is large compared with the shelf width and applies to most midlatitude shelves. The approximation can be poor on some shelves even in midlatitude (see e.g. Schulz, Mied & Snow 2012). Relaxing the rigid-lid approximation introduces a Kelvin wave, present at all frequencies, and super-inertial Poincaré waves. This means that

https://doi.org/10.1017/jfm.2020.656 Published online by Cambridge University Press

the continuous spectrum of the wave operator is no longer bounded so either energy leaks into the Kelvin wave and no tCSWs exist or, if tCSWs exist, they are embedded in the continuous spectrum. These lead to a distinctly different and more challenging analytical problem.

It is the purpose of this work to show that tCSWs can indeed exist for a non-rectilinear shelf geometry even in the presence of a free surface. Section 2 formulates the problem and § 3 considers rectilinear shelves to establish the non-rectilinear shelf geometry that can lead to trapping. By employing a simple but efficient numerical method, it is shown that changing the slope across the shelf (i.e. a submerged ridge) raises the cutoff frequency for CSWs and thus can lead to trapping. The asymptotic method is presented in § 4 where the shelf is modelled as a waveguide, by approximating the shelf–ocean boundary as a rigid wall. The topography chosen varies slowly along the shelf, so the scale of the alongshelf variations of the isobaths is large compared with the shelf's width. A regular asymptotic expansion leads to a hierarchy of equations, where the problem is reduced to finding the solutions of a second-order differential equation in the alongshelf direction. The rigid-lid case is also summarised since it follows immediately from our analysis. Subsequently it is shown that a submerged ridge can support trapped modes while a submerged valley does not. The accuracy of the asymptotic method is demonstrated by employing a highly accurate pseudospectral method that solves the full equation and demonstrates that the results of both methods are in close agreement. In § 5 we consider a non-rectilinear shelf that abuts to open ocean, thus eliminating the approximate b.c. at the shelf–ocean boundary. The trapping of CSWs is shown numerically, and it also shown that the frequency of trapping, when considering an open-ocean geometry, is bounded below by the respective frequency of a trapped mode when the approximate b.c. at the shelf–ocean boundary is considered. Finally, a brief discussion of our results is given in § 6.

## 2. Formulation of the problem

The linearised shallow water equations can be written as

$$u_t - fv = -g\eta_x, \tag{2.1}$$

$$v_t + fu = -g\eta_y, \tag{2.2}$$

$$\eta_t + (uH)_x + (vH)_y = 0, \tag{2.3}$$

where $f$ is the Coriolis parameter (assumed constant), $g$ is the gravitational acceleration, $u(x, y, t)$ and $v(x, y, t)$ are the components of the horizontal velocity, $\eta(x, y, t)$ is the free-surface displacement and $H(x, y)$ is the undisturbed fluid depth. Equations (2.1)–(2.3) can be rearranged to give an equation for $\eta$ alone (see e.g. LeBlond & Mysak 1978),

$$(\partial_{tt} + f^2)\eta_t - g\boldsymbol{\nabla}\cdot(H\boldsymbol{\nabla}\eta_t) + gf\hat{\boldsymbol{z}}\cdot(\boldsymbol{\nabla}\eta\times\boldsymbol{\nabla}H) = 0. \tag{2.4}$$

Taking the coastline as impermeable gives the b.c.

$$\eta_{yt} - f\eta_x = 0, \quad y = 0, \tag{2.5}$$

and the full problem, solved numerically in § 5, has the open-ocean b.c.

$$\eta \to 0, \quad y \to \infty. \tag{2.6a,b}$$

https://doi.org/10.1017/jfm.2020.656 Published online by Cambridge University Press

This is approximated in § 4 by taking the shelf–ocean boundary to be impermeable, so

$$\eta_{yt} - f\eta_x = 0, \quad y = 1. \tag{2.7}$$

In the rigid-lid case, using the stream function formulation, Johnson (1989) has shown that demanding that the normal component of the velocity vanishes at the shelf–ocean boundary gives a lower bound to the frequency of trapping, which is accurate in the short-wave limit. Even though no analogous result exists for the free-surface formulation, the approximate b.c. (2.7) gives a clearer problem to deal with for the asymptotic method, allowing explicit solutions to be derived for simple topographies in the rigid-lid case. Note that, this b.c. admits a Kelvin wave (also present at all frequencies) propagating along the outer wall in the opposite direction of the rest of the waves considered here, and thus does not interact with them.

For periodic solutions of the form

$$\eta = \mathrm{Re}\{\Phi(x, y)\exp(-\mathrm{i}\omega ft)\}, \tag{2.8}$$

(2.4) reduces to

$$\omega\nabla\cdot(H\nabla\Phi) - \mathrm{i}\hat{z}\cdot(\nabla\Phi\times\nabla H) + [(\omega^3-\omega)/R^2]\Phi = 0, \tag{2.9}$$

where $\omega$ is the non-dimensional frequency, $R = \sqrt{gH_m}/fL$ is the non-dimensional parameter which gives the ratio of the Rossby radius of deformation to the shelf width L and $H_m$ is the dimensional depth at the ocean. All depths are scaled to $H_m$. The depth profile $H$ has been scaled to equal 1 at the deepest end and is constant in the ocean region $y > 1$. Equation (2.9) is a cubic eigenvalue problem for the eigenvalue $\omega$ which also appears in the b.c.s (2.5) and (2.7). For low frequency modes where $\omega \ll 1$, the term $\omega^3$ can be neglected to give a linear eigenvalue problem (Rhines 1969). This also removes the Poincaré waves from the problem, however, this reduction is not necessary in the methods presented here.

## 3. Rectilinear shelf geometries

For any mode to become trapped, the geometry of the shelf must change along the shelf in such a way that CSWs can propagate at a higher frequency (locally) compared with the far field. For a rectilinear shelf, i.e. of the form $H \equiv H(y)$, the spectrum of the operator in (2.9) subject to the b.c.s (2.5) and (2.7) or (2.6*a*,*b*) is purely continuous and has no trapped modes (Huthnance 1975). However, in order to understand the nature of the spectrum of operator (2.9), with respect to shelf geometry changes, it is thus convenient to consider initially rectilinear shelves. Introducing $\Phi = Y(y)\exp(\mathrm{i}kx)$, where $k$ is the $x$-wavenumber, gives from (2.9) and (2.5)–(2.6*a*,*b*), for the channel model with rigid walls,

$$(HY')' + [kH'/\omega - k^2H + (\omega^2-1)/R^2]Y = 0, \tag{3.1}$$

$$\omega Y' + kY = 0, \quad y = 0, \tag{3.2}$$

$$\omega Y' + kY = 0, \quad y = 1. \tag{3.3}$$

For the full model the shelf-ocean b.c (3.3) is replaced by the open-ocean condition

$$Y \to 0, \quad y \to \infty. \tag{3.4a,b}$$

This one-dimensional problem can be easily solved with a highly accurate spectral, Chebyshev discretisation similarly to Kaoullas & Johnson (2010*a*). Appendix A gives

https://doi.org/10.1017/jfm.2020.656 Published online by Cambridge University Press

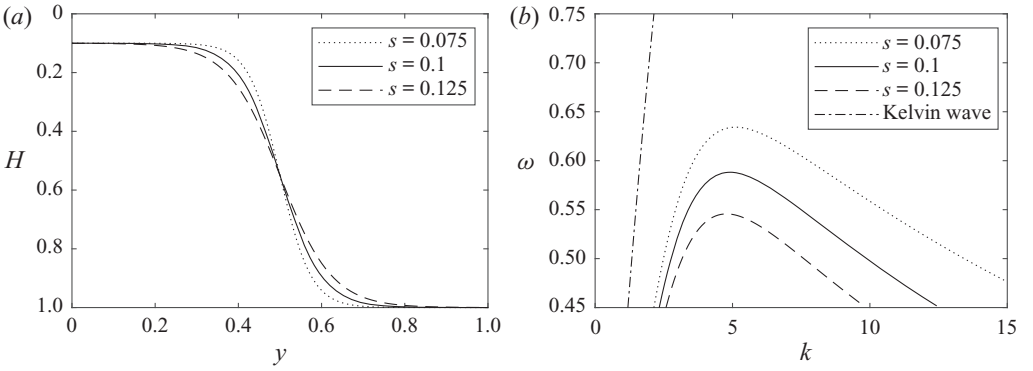



FIGURE 1. (*a*) Depth profiles and (*b*) dispersion curves of the first propagating mode and the Kelvin mode for various shelf slopes for the profile (3.5). Here, $c = 0.5$, $H_0 = 0.1$ and $R = 1$.

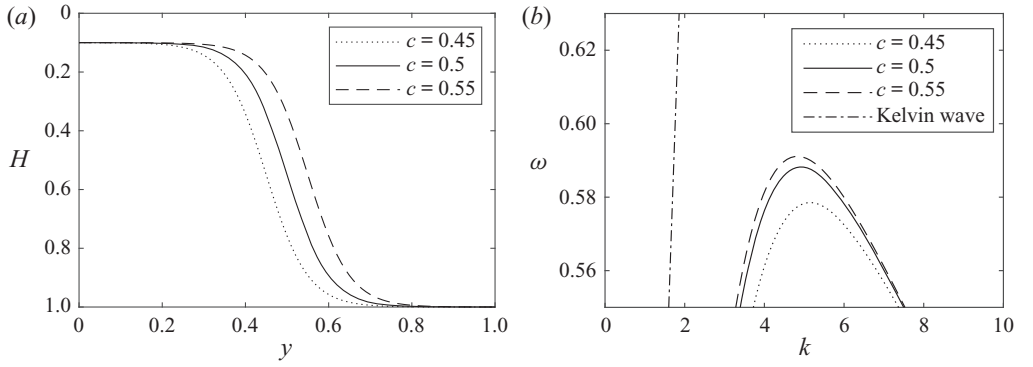



FIGURE 2. (*a*) Depth profiles and (*b*) dispersion curves of the first propagating mode and the Kelvin mode for various shelf breaks for the profile (3.5). Here, $s = 0.1$, $H_0 = 0.1$ and $R = 1$.

the details. The open-ocean b.c. can be replaced with a nonlinear b.c. at the shelf–ocean boundary, however, for simplicity we will use a smooth topography function and extend the flat ocean sufficiently for offshore modes to decay. It is shown in Kaoullas & Johnson (2012), that for the rigid-lid case, locally changing the shelf slope or the distance of the shelf break from the coast can lead to trapped CSWs. Thus for the free-surface case consider the (rather more general) depth profile

$$H(y) = H_0 + (1 - H_0)\{1 + \tanh[(y - c)/s]\}/2, \tag{3.5}$$

where, $c$ is the distance of the shelf break from the coast, $s$ is the slope of the shelf and $H_0$ the depth at the coast (for sufficiently large $c/s$). Figure 1 shows (for the open-ocean model) that if the slope of the shelf increases, so too does the frequency at which waves can propagate. Similarly, as can be seen in figure 2, increasing the distance of the shelf break from the coast results in higher frequency of propagation. Trapping is thus possible although not proven. The coastal Kelvin wave is also present at all frequencies (almost unaffected by the change in shelf slope), implying that any tCSWs are embedded in the continuous spectrum. The same result is obtained for a channel with solid wall geometry (omitted here).

https://doi.org/10.1017/jfm.2020.656 Published online by Cambridge University Press

## 4. Asymptotic method

### 4.1. *Slowly and slightly varying shelf geometry*

The geometry here is the straight channel $0 \leq y \leq 1$, $-\infty \leq x \leq \infty$. Consider a non-rectilinear shelf such that, parallel to the channel the shelf depth changes only slowly and by a small amount with distance along the shelf, i.e. $H(\epsilon x, y) = H(\xi, y)$, where $\epsilon$ is a small dimensionless parameter representing the ratio of the shelf width to the scale of the longitudinal variation in offshore depth profile. It is possible to avoid the slightly varying approximation using the WKB method and solve the one-dimensional eigenvalue, cross-stream problem, at each station along the shelf, similarly to Rodney & Johnson (2015) and Rocha *et al.* (2020) numerically, however, the slight variation employed here allows the alongstream structure to be obtained analytically. In the new coordinates $(\xi, y)$ the governing equation (2.9) and b.c.s (2.5) and (2.7) become

$$\omega[H(\epsilon^2\Phi_{\xi\xi} + \Phi_{yy}) + (\epsilon^2 H_\xi \Phi_\xi + H_y\Phi_y)] + \epsilon \mathrm{i}(H_\xi\Phi_y - H_y\Phi_\xi) + [(\omega^3 - \omega)/R^2]\Phi = 0, \tag{4.1}$$

$$\mathrm{i}\omega\Phi_y + \epsilon\Phi_\xi = 0, \quad y = 0, \tag{4.2}$$

$$\mathrm{i}\omega\Phi_y + \epsilon\Phi_\xi = 0, \quad y = 1. \tag{4.3}$$

We now make the following regular asymptotic expansion:

$$\Phi \sim \exp(\mathrm{i}\mu\xi/\epsilon)\Psi, \quad \Psi = f_0(\xi)\Psi^c(y) + \epsilon\Psi_1(\xi, y) + \epsilon^2\Psi_2(\xi, y) + \cdots, \tag{4.4a,b}$$

$$\omega = \omega_0 + \epsilon\omega_1 + \epsilon^2\omega_2 + \cdots, \tag{4.5}$$

where $\omega_0$ is the cutoff frequency, $\Psi^c(y)$ the corresponding solution to the one-dimensional problem, $f_0(\xi)$ is the alongstream solution (i.e. the envelope) and $\mu$ is the $x$-wavenumber at the cutoff frequency, i.e. the maximum frequency of propagation as a function of the alongshore wavenumber. Expansion (4.5) differs from those in Postnova & Craster (2008) and Kaoullas & Johnson (2012), which are expansions in powers of the reciprocal of the frequency.

The strategy here is to obtain a hierarchy of equations where, to leading order, the cross-stream structure of the modes for a rectilinear shelf are determined, and to second order, the mechanisms of trapping are given by a second-order ordinary differential equation for $f_0(\xi)$ (see below). Readers who want to skip the mathematical details can proceed to §§ 4.3 and 5. Substituting the first of (4.4*a*,*b*) into (4.1)–(4.3) we get

$$\epsilon^2\Psi_{\xi\xi} + \Psi_{yy} + \left(\epsilon^2\frac{H_\xi}{H} - \epsilon\frac{\mathrm{i}}{\omega}\frac{H_y}{H} + \epsilon 2\mathrm{i}\mu\right)\Psi_\xi + \left(\frac{H_y}{H} + \epsilon\frac{\mathrm{i}}{\omega}\frac{H_\xi}{H}\right)\Psi_y + \left(\epsilon\mathrm{i}\mu\frac{H_\xi}{H} + \frac{\mu}{\omega}\frac{H_y}{H} - \mu^2 + \frac{\omega^2 - 1}{HR^2}\right)\Psi = 0, \tag{4.6}$$

$$\mathrm{i}\omega\Psi_y + \mathrm{i}\mu\Psi + \epsilon\Psi_\xi = 0, \quad y = 0, 1. \tag{4.7}$$

The expansion simplifies for the exponential depth profile

$$H(x, y) = \exp(2bp(\xi, y)), \quad y \in [0, 1], \tag{4.8}$$

https://doi.org/10.1017/jfm.2020.656 Published online by Cambridge University Press

where

$$p(\xi, y) = (\, y - 1 + y(1 - y)\alpha\epsilon^2\gamma(\xi)), \tag{4.9}$$

$$p_y = 1 + (1 - 2y)\alpha\epsilon^2\gamma(\xi), \quad p_\xi = y(1 - y)\alpha\epsilon^2\gamma_\xi(\xi), \tag{4.10a,b}$$

corresponding to a submerged ridge for $\alpha < 0$ (figure 3*a*) and a submerged valley for $\alpha > 0$ (figure 3*b*). For convenience the amplitude of the change in depth profile along $\xi$, in (4.8), has been scaled to $\epsilon^2$ (while the slow variation is of order $\epsilon$) so that the variation in $\xi$ would only appear to order $\epsilon^2$ and thus the geometry now is more slight than slow. Then (4.6) becomes

$$\epsilon^2\Psi_{\xi\xi} + \Psi_{yy} + (\epsilon^2 2bp_\xi + \epsilon 2\mathrm{i}(\mu - bp_y/\omega))\Psi_\xi + 2b(\, p_y + \epsilon\mathrm{i}p_\xi/\omega)\Psi_y$$
$$+ (\epsilon 2bi\mu p_\xi + 2b\mu p_y/\omega - \mu^2 + (\omega^2 - 1)/(HR^2))\Psi = 0. \tag{4.11}$$

Now

$$\omega^3 - \omega = \omega_0^3 - \omega_0 + \epsilon\omega_1(3\omega_0^2 - 1) + \epsilon^2(3\omega_0\omega_1^2 + 3\omega_0^2\omega_2 - \omega_2) + O(\epsilon^3), \tag{4.12}$$

and the Taylor series expansion of the reciprocal of the depth profile is

$$H^{-1}(\xi, y) = \mathrm{e}^{2b(1-y)}(1 - \epsilon^2 2by(1 - y)\alpha\gamma(\xi) + O(\epsilon^4)), \tag{4.13}$$

giving the leading-order equation

$$(h\Psi_y^c)_y + [2b\mu/\omega_0 - \mu^2 + (\omega_0^2 - 1)/(hR^2)]h\Psi^c = 0, \tag{4.14}$$

$$\omega_0\Psi_y^c + \mu\Psi^c = 0, \quad y = 0, 1, \tag{4.15}$$

where $h(\, y) = \exp(2b(\, y - 1))$. Equation (4.14) with b.c.s (4.15) is to be solved numerically using the numerical method introduced in Appendix A. Solutions are normalised by requiring

$$\int_0^1 h\Psi^{c2}\,\mathrm{d}y = 1. \tag{4.16}$$

Multiplying (4.14) by $\Psi^c$, integrating over $y \in [0, 1]$ and using (4.15) gives the dispersion relation,

$$-k_0[h\Psi^{c2}]_0^1 - \omega_0\int_0^1 h\Psi_y^{c2}\,\mathrm{d}y + 2bk_0 - \omega_0 k_0^2 + (\omega_0^3 - \omega_0)/R^2\int_0^1 \Psi^{c2}\,\mathrm{d}y = 0, \tag{4.17}$$

on setting $\mu = k_0$, the $x$-wavenumber at the cutoff frequency, $\omega_0$, of the rectilinear channel ($\epsilon = 0$). Differentiating (4.17) with respect to $k_0$ and setting the group velocity to zero gives

$$2b - \left[h\Psi^{c2}\right]_0^1 = 2k_0\omega_0 = 2\mu\omega_0. \tag{4.18}$$

Unlike the rigid-lid case (Kaoullas & Johnson 2012; Rodney & Johnson 2015), the bracketed term in (4.18) is non-zero; this proves crucial below. At the next order

$$(h\Psi_{1_y})_y + [2b\mu/\omega_0 - \mu^2 + (\omega_0^2 - 1)/(hR^2)]h\Psi_1 + 2\omega_1(\omega_0/(hR^2)$$
$$- b\mu/\omega_0^2)hf_0\Psi^c + 2\mathrm{i}(\mu - b/\omega_0)hf_{0_\xi}\Psi^c = 0, \tag{4.19}$$

https://doi.org/10.1017/jfm.2020.656 Published online by Cambridge University Press

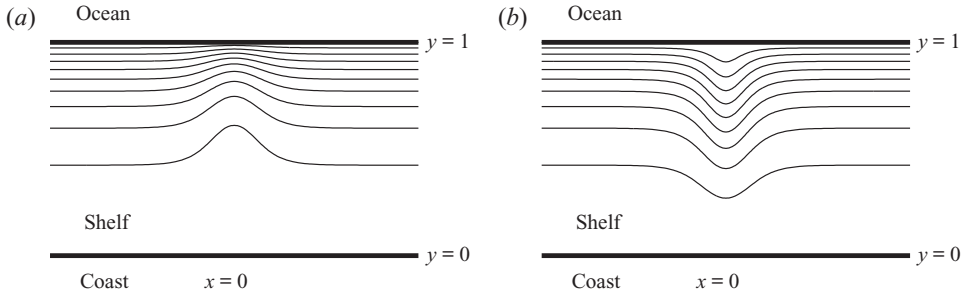



FIGURE 3. Isobaths (not drawn to scale) of (*a*) a submerged ridge ($\alpha < 0$) and (*b*) a submerged valley ($\alpha > 0$).

$$\mathrm{i}\omega_0\Psi_{1_y} + \mathrm{i}\mu\Psi_1 + \mathrm{i}\omega_1 f_0\Psi^c_y + f_{0_\xi}\Psi^c = 0, \quad y = 0, 1, \tag{4.20}$$

where $f_0(\xi)$ is the alongstream structure of the solution (see (4.4*a*,*b*)) which needs to be determined. Multiplying (4.19) by $\Psi^c$ and integrating over $y \in [0, 1]$ gives

$$\left[h\Psi_{1_y}\Psi^c - h\Psi_1\Psi^c_y\right]^1_0 + \frac{2\omega_1}{\omega_0}f_0\left(\frac{\omega_0^2}{R^2}\int_0^1 \Psi^{c2}\,\mathrm{d}y - \frac{b\mu}{\omega_0}\right) + 2\mathrm{i}\left(\mu - \frac{b}{\omega_0}\right)f_{0_\xi} = 0. \tag{4.21}$$

Using (4.18) and the b.c.s (4.15) and (4.20), equation simplifies (4.21) to

$$2\omega_1 f_0\left(\frac{\omega_0}{R^2}\int_0^1 \Psi^{c2}\,\mathrm{d}y - \frac{\mu^2}{\omega_0}\right) = 0. \tag{4.22}$$

For a non-trivial solution $f_0$ is non-zero, so either $\omega_1 = 0$ or the bracketed term in (4.22) vanishes. As can be seen from figure 4, for all values of $b > 0$ and $R > 0$, the term in the brackets is non-zero which forces $\omega_1 = 0$. It remains to determine $\Psi_1$, from

$$\Psi_{1_{yy}} + 2b\Psi_{1_y} + [2b\mu/\omega_0 - \mu^2 + (\omega_0^2 - 1)/(hR^2)]\Psi_1 = -2\mathrm{i}\,(\mu - b/\omega_0)f_{0_\xi}\Psi^c, \tag{4.23}$$

$$\omega_0\Psi_{1_y} + \mu\Psi_1 = \mathrm{i}f_{0_\xi}\Psi^c, \quad y = 0, 1. \tag{4.24}$$

This is a non-homogeneous ordinary differential equation with solution

$$\Psi_1 = f_1(\xi)\Psi^c + M(y)f_{0_\xi}, \tag{4.25}$$

where $M$ is to be determined. Substituting (4.25) into (4.23) and (4.24) we get an ordinary differential equation for $M$ as follows:

$$M_{yy} + 2bM_y + [2b\mu/\omega_0 - \mu^2 + (\omega_0^2 - 1)/(hR^2)]M = -2\mathrm{i}\,(\mu - b/\omega_0)\,\Psi^c, \tag{4.26}$$

$$\omega_0 M_y + \mu M = \mathrm{i}\Psi^c, \quad y = 0, 1. \tag{4.27}$$

Since $\omega_0$, $\mu$ and $\Psi^c$ have been determined, through (4.14), (4.15) and (4.18), equation (4.26) can be solved straightforwardly numerically as a non-homogeneous, linear system of equations. To double precision the resulting matrix is ill-conditioned, and thus required higher precision using the Advanpix (2019) multiprecision toolkit for Matlab. The order

https://doi.org/10.1017/jfm.2020.656 Published online by Cambridge University Press

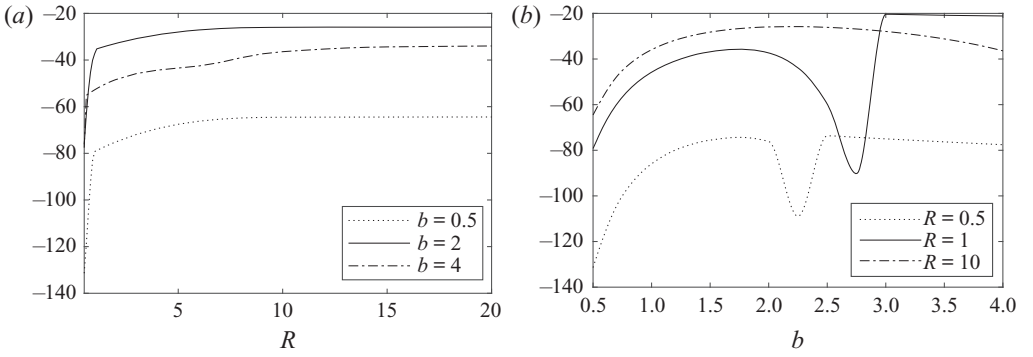



FIGURE 4. The bracketed term in (4.22) computed numerically for (*a*) $b$ fixed against various values of $R$ and (*b*) $R$ fixed against various values of $b$.

$\epsilon^2$ equation is

$$(h\Psi_{2_y})_y + [2b\mu/\omega_0 - \mu^2 + (\omega_0^2 - 1)/(hR^2)]h\Psi_2 + 2\omega_2(\omega_0/(hR^2) - b\mu/\omega_0^2)h\Psi^c f_0 + hf_{0_{\xi\xi}}\Psi^c + 2\mathrm{i}(\mu - b/\omega_0)h\Psi_{1_\xi} + 2b\alpha\gamma h[(1-2y) \times (\Psi_y^c + (\mu/\omega_0)\Psi^c) - y(1-y)(\omega_0^2 - 1)/(hR^2)\Psi^c]f_0 = 0, \tag{4.28}$$

$$\mathrm{i}\omega_0\Psi_{2_y} + \mathrm{i}\mu\Psi_2 + \mathrm{i}\omega_2 f_0\Psi_y^c + \Psi_{1_\xi} = 0, \quad y = 0, 1. \tag{4.29}$$

Multiplying (4.28) by $\Psi^c$ and integrating gives

$$I_1 f_{0_{\xi\xi}} + V(\xi)f_0 = \omega_2 I_2 f_0, \tag{4.30}$$

where

$$V(\xi) = \alpha 2b\gamma(\xi)\left(\int_0^1 h(1-2y)(\Psi^c\Psi_y^c + (\mu/\omega_0)\Psi^{c2})\,\mathrm{d}y - \frac{\omega_0^2 - 1}{R^2}\int_0^1 y(1-y)\Psi^{c2}\,\mathrm{d}y\right), \tag{4.31}$$

$$I_1 = 1 + \frac{\mathrm{i}}{\omega_0}[hM\Psi^c]_0^1 + 2\mathrm{i}\left(\mu - \frac{b}{\omega_0}\right)\int_0^1 hM\Psi^c\,\mathrm{d}y, \tag{4.32}$$

$$I_2 = \frac{2}{\omega_0}\left(\mu^2 - \frac{\omega_0^2}{R^2}\int_0^1 \Psi^{c2}\,\mathrm{d}y\right). \tag{4.33}$$

Equation (4.30) is a one-dimensional Schrödinger equation with $V$ the associated potential and $\omega_2$ the eigenvalue. It can be determined numerically, similarly to figure 4 (not shown here), that $I_1 > 0$ and the term in the brackets in (4.31) is negative. For a trapped mode to exist, its frequency must lie above the cutoff frequency of the unperturbed channel and so from (4.5), $\omega_2$ is positive. Following Gridin *et al.* (2005), multiplying both sides of (4.30)

https://doi.org/10.1017/jfm.2020.656 Published online by Cambridge University Press

by $f_0$ and integrating by parts on $\xi \in (-\infty, \infty)$ gives

$$-I_1 \int_{-\infty}^{\infty} (f_{0_\xi})^2 \, \mathrm{d}\xi + \int_{-\infty}^{\infty} V(\xi)\,(f_0)^2 \, \mathrm{d}\xi = I_2\omega_2 \int_{-\infty}^{\infty} (f_0)^2 \, \mathrm{d}\xi, \tag{4.34}$$

where we have used the requirement for trapped modes, that $f_0$ vanishes at infinity. If the second integral in (4.34) is negative, i.e. $V < 0$, the left-hand side of (4.34) becomes negative, forcing $\omega_2$ to be negative (since $I_2$ is positive from figure 4), thus no trapping is possible. Hence if $V$ is positive, trapped modes might exist (depending on the magnitude of $V$).

In the rigid-lid case, i.e. $R \to \infty$, closed form solutions exist for the depth profile (4.8). The analysis is identical to § 4.1 and so we refer the reader to appendix B for the derivation of these solutions.

### 4.2. *Analytical solution*

Choosing $\gamma(\xi) = \mathrm{sech}^2(\xi)$, allows (4.30) to be solved analytically following Landau & Lifshitz (1991) as

$$f_0(\xi) = \cosh^{m-s}(\xi) F\left(-m;\, 2s+1-m;\, s+1-m;\, (1-\tanh\xi)/2\right), \tag{4.35}$$

where

$$s = (\sqrt{1+4\alpha\beta} - 1)/2, \quad \omega_2 = (s-m)^2 I_1/I_2, \quad 0 \le m < s, \tag{4.36a,b}$$

and $F$ is the confluent hypergeometric function of degree m. Here $-m$ is a positive integer, and so $F$ is a polynomial of degree $m$ with $\beta$ given by

$$\beta = \begin{cases} -2b & \text{rigid-lid,} \\ V/I_1 & \text{full problem,} \end{cases} \tag{4.37}$$

for $V$ and $I_1$ given by (4.31) and (4.32), respectively. The condition that $s > m$ gives the lower bound on the parameter $\alpha$:

$$-\alpha > [(2m-1)^2 - 1]/4\beta. \tag{4.38}$$

For the first transverse mode ($m = 1$) to become trapped, condition (4.38) requires simply that $\alpha < 0$. Thus, provided there is a perturbation in depth leading to a submerged ridge, i.e. $\alpha < 0$, the first alongshelf mode is trapped. The corresponding cross-shelf mode number is arbitrary, leading to a countably infinite set of trapped modes. For higher alongshore modes to get be trapped, a larger value of $|\alpha|$ is required, corresponding to a larger magnitude of the potential $V$ and hence to a larger amplitude in the depth perturbation.

### 4.3. *Numerical method and results*

The full equation (4.6) with b.c.s (4.7), can be written as

$$\begin{aligned} &\omega^4/(HR^2)\Psi + \omega^2(\Psi_{xx} + \Psi_{yy} + 2b(p_x\Psi_x + p_y\Psi_y) - 1/(HR^2)\Psi) \\ &\quad + \omega 2b\mathrm{i}([1-p_y]\Psi_x + p_x\Psi_y + bp_x\Psi) + b^2(2p_y - 1)\Psi = 0, \end{aligned} \tag{4.39}$$

$$\omega^2\Psi_y - \mathrm{i}\omega\Psi_x + b\Psi = 0, \quad y = 0,\, 1, \tag{4.40}$$

using the relation $\mu = b/\omega$ to eliminate (most of) the phase from the fast carrier wave in the alongstream direction. This relation is exact for the rigid-lid problem (hence all of

https://doi.org/10.1017/jfm.2020.656 Published online by Cambridge University Press

the phase is removed) and a good approximation for the full problem (compared with the analogue of (4.18)). This slight approximation for the full problem allows stable numerical computations and, with most of the rapid phase variation removed, requires much smaller matrices to accurately solve the eigenvalue problem. A highly accurate pseudospectral method was employed, with a Chebyshev grid discretisation in the cross-stream direction and a Hermite grid in the alongstream direction. When dealing with unbounded domains the accuracy of the solution is greatly improved with the appropriate choice of a scale factor (Tang 1993; Weideman & Reddy 2000; Shen & Wang 2009) so that the largest collocation point lies where the solution is smaller than a desired value (see Kaoullas & Johnson (2012), for more details). Appendix C gives details on linearising this polynomial eigenvalue problem (4.39), for the eigenvalue $\omega$, to a generalised eigenvalue problem and imposing the b.c.s (4.40). The linearisation of any polynomial eigenvalue problem is not unique and the associated backwards error is an open topic of research (Tisseur 2000). The choice here leads to reasonably conditioned matrices.

Let $\omega_{m,n}$ denote the frequency of the $(m, n)$ tCSW, where $m$ is the alongshore mode number and $n$ the cross-shelf mode number so that $m = 1$ corresponds to the fundamental mode. Table 1 shows the accuracy of the asymptotic method, when compared with the numerical solution of (4.6), for the rigid-lid and the full problem. In particular, the accuracy of $\omega_2$ which is the next order correction to the cutoff frequency of the asymptotic method ($\omega_2^A$), is assessed by comparing it with the numerically determined value $\omega_2^N = (w^N - w_0)/\epsilon^2$. The relative error of the asymptotic eigenfrequencies is well below 2 %, implying that the asymptotic solution is accurate. This accuracy is also demonstrated in figure 5 where the absolute value of $\Psi$ is plotted as a function of $\xi$ at $y = 0$. The maximum of the disturbance is concentrated at the maximum amplitude of the isobath deviation, i.e. at $\xi = 0$ and then decays exponentially in the far field as $\exp(-k_r\xi)$ where $k_r$ is the real part of the wavenumber of the corresponding decaying mode in the far field.

These tCSWs all lie within the continuous spectrum and since they decay to zero exponentially in the far field, no energy leaks from the region of trapping. To demonstrate that they do not project to the Kelvin wave, note the orthogonality relation (Proudman 1929)

$$\iint H(u_i u_j + v_i v_j)\,\mathrm{d}x\,\mathrm{d}y + \frac{1}{R^2}\iint \eta_i \eta_j\,\mathrm{d}x\,\mathrm{d}y = \delta_{i,j}E_j, \tag{4.41}$$

where $u_l$, $v_l$, $\eta_l$, for $l = i, j$ are the horizontal velocities and the surface displacement, respectively, for any two solutions of (2.9) subject to the b.c.s (2.5) and (2.7), $E_i$ is twice the energy associated with the $i$-th mode which is given by (4.41) with $j = i$ with the integrals evaluated over the channel. Substituting the Kelvin wave (that is concentrated along the coast) and the trapped CSW into (4.41), and evaluating the integrals numerically gives that the right-hand side of (4.41) is $O(10^{-10})$ which implies that the trapped mode is orthogonal to the Kelvin wave.

## 5. Open ocean

It has been shown in this work that CSWs can be trapped for an infinitely long channel of variable bathymetry. In order to extend these results to an open ocean and also check the validity of the approximate condition at the shelf–ocean boundary, the full equation (2.9)

https://doi.org/10.1017/jfm.2020.656 Published online by Cambridge University Press

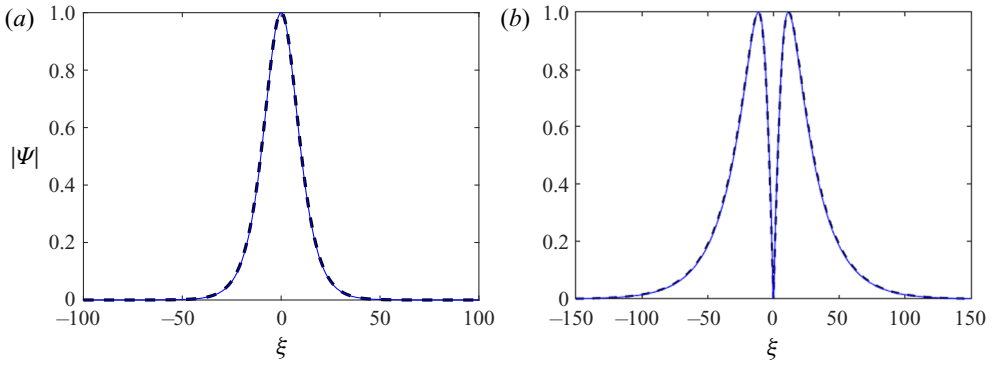



FIGURE 5. The envelope of the pressure fluctuations, $|\Psi|$, as a function of $\xi$ at $y = 0$ generated by the numerical method (solid line) and the asymptotic method (dashed line) for the (1,1) and (2,1) modes, for the full problem for parameters $b = 2$, $\alpha = -1.5$ and $\epsilon = 0.1$.

| | $m$ | $n$ | $\omega$ | $\omega_2^A$ | $\omega_2^N$ | r.error |
|---|---|---|---|---|---|---|
| Rigid lid | 1 | 1 | 0.5378100300 | 0.077439 | 0.078075 | 0.008 |
| | 2 | 1 | 0.5372238862 | 0.019359 | 0.019461 | 0.005 |
| Full problem | 1 | 1 | 0.4652203924 | 0.039325 | 0.039994 | 0.016 |
| | 2 | 1 | 0.4648646366 | 0.004336 | 0.004418 | 0.018 |

TABLE 1. The trapped frequencies $\omega$ as calculated from the asymptotic method and a comparison of $\omega_2$ from the asymptotic method, $\omega_2^A$, and the numerical method, $\omega_2^N$. Here $\alpha = -1.5$, $b = 2$ and $\epsilon = 0.1$.

subject to the b.c.s (2.5) and (2.6*a*,*b*) is solved numerically. Consider the depth profile,

$$H(x, y) = \begin{cases} 1 - (1 - H_0)\exp(-(y^2 - p(x)^2)^{-s} + p(x)^{-2s}), & 0 \le y \le p(x), \\ 1, & y \ge p(x), \end{cases} \tag{5.1}$$

where $p(x) = (1 + \alpha\epsilon^2 \mathrm{sech}^2 \epsilon x)/(1 + \alpha)$. The depth at the coast is $H_0$ and the depth in the ocean is 1. Here $\alpha > 0$ corresponds to the submerged ridge case and $\alpha < 0$ to the submerged valley case. The numerical method of Appendix A shows that only the submerged ridge topography admits trapped modes. For the numerical method here, a Hermite interpolant is employed in the $x$ direction and a Laguerre interpolant in the $y$ direction. This cubic eigenvalue problem is linearised and the b.c.s are imposed following appendix C.

Trapping of the $\omega_{1,1}$ and $\omega_{2,1}$ trapped modes is shown in figure 6. Most of the wave disturbance is concentrated along the submerged ridge and the modes decay in the far field both along and away from the coast. The approximate b.c. (2.7), which enabled the reduction of the problem to a channel with solid walls in § 4, is evaluated by imposing this b.c. at $y = L_y$, by using a Chebyshev interpolant in the cross-shore direction. We set $L_y = \max P(x)$, which corresponds to the shelf–ocean boundary, and then gradually increase $L_y$ to infinity, which should imply that the frequency of tapping, $\omega_L$, should converge to the frequency of trapping, $\omega$, for the unapproximated open-ocean b.c. We also

https://doi.org/10.1017/jfm.2020.656 Published online by Cambridge University Press

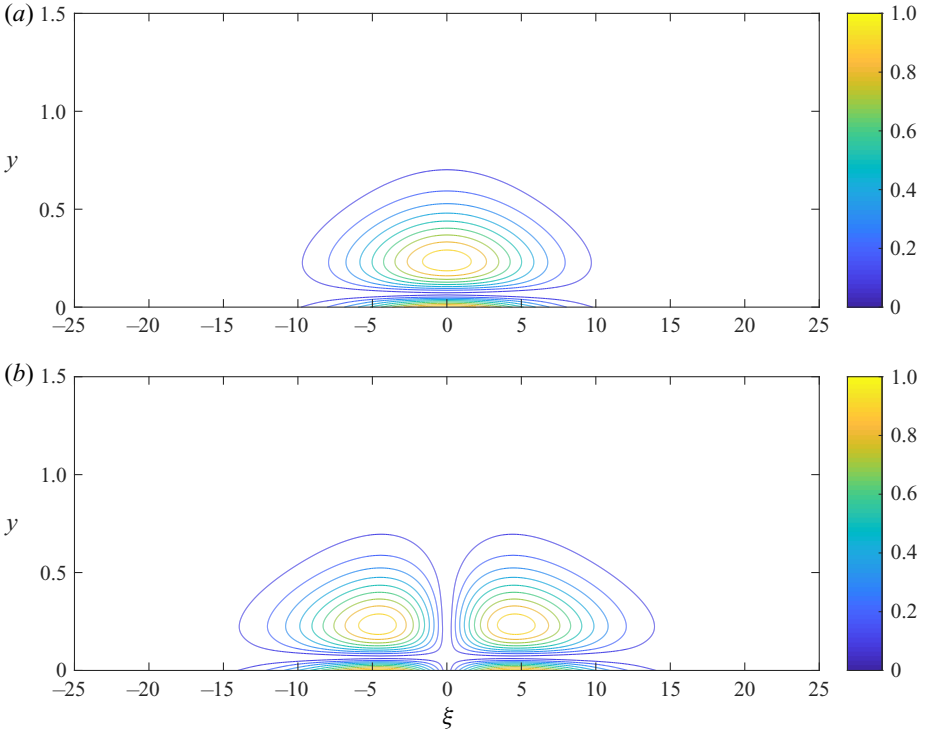



FIGURE 6. The stream function amplitude, $|\Psi|$ of (*a*) the (1,1) mode and (*b*) the (2,1) mode for the open-ocean case. Here, $b = 2$, $\alpha = 0.2$ and $\epsilon = 0.1$.

investigate whether demanding that the tangential velocity vanishes at the shelf–ocean boundary, i.e. $\mathrm{i}\omega\eta_x - \eta_y = 0$, can also serve as an approximate b.c. (with corresponding frequency of trapping denoted by $\omega_U$). For the rigid-lid case it is known that these two approximations at the shelf–ocean boundary (requiring the normal or the tangential component of the velocity to vanish) give a lower and an upper bound to the frequency of trapping (Johnson 1989; Kaoullas & Johnson 2012). Denote the scaled (lower and upper) frequencies of trapping by $\hat{\omega}_i = \omega_i/\omega - 1$, $i = L, U$, and $\hat{\omega} = 0$ is the (scaled) frequency of the unapproximated problem. It is demonstrated in figure 7 that both $\hat{\omega}_L$ and $\hat{\omega}_U$ converge to $\hat{\omega}$ as $L_y$ increases. Thus, similarly to the rigid-lid case, we have the following bounds to the frequency of trapping:

$$\omega_L \leq \omega \leq \omega_U. \tag{5.2}$$

## 6. Discussion

It is well known that in the rigid-lid limit (Kaoullas & Johnson 2012; Rodney & Johnson 2015) alongshore variations in the topography can lead to CSWs being trapped both away and along the coast. Here, a regular asymptotic expansion method has been presented to investigate whether similar shelf geometries can still support tCSWs when the rigid-lid assumption is relaxed. Mathematically, this is a nonlinear eigenvalue problem for the spectral parameter, that is the frequency, $\omega$, which also appears in the b.c.s. The presence of the Kelvin wave at all frequencies implies that the spectrum of the operator is everywhere continuous and if any trapped mode exists, it will be embedded in the continuous spectrum (similarly to the water wave problem in Aslanyan *et al.* (2000)).

https://doi.org/10.1017/jfm.2020.656 Published online by Cambridge University Press

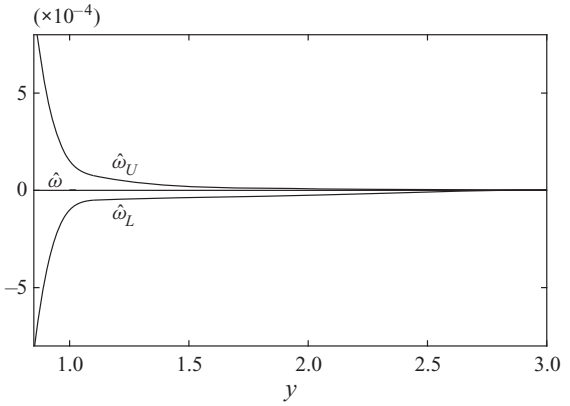



FIGURE 7. Lower ($\hat{\omega}_L$) and upper bounds ($\hat{\omega}_U$) for the frequency of trapping $\hat{\omega}$ of the (1,1) mode for increasing $L_y$.

A waveguide with impermeable sidewalls is considered and the scale of the alongshelf variations of the isobaths is taken to be large, compared with the shelf width. It is shown that in the case of a submerged ridge, trapping is always possible even when the depth is perturbed only slightly while in the case of a submerged valley, no trapping is possible. The rigid-lid case follows immediately and it is shown that the frequencies of trapping for the pressure formulation here are in excellent agreement with the stream function formulation of Kaoullas & Johnson (2012) and Rodney & Johnson (2015). The accuracy of this method is demonstrated by comparing the asymptotic results with the numerical results of a pseudospectral method, which shows that the asymptotic method is extremely accurate. Additionally, the numerical method is also used to demonstrate that trapped modes continue to exist when the shelf extends into the open ocean, thus removing the approximation taken at the shelf–ocean boundary.

It is generally accepted that the main mechanism of excitation of CSWs is the wind stress (see Adams & Buchwald 1969) of a comparable period. In the rigid-lid limit, it has been shown in Rodney & Johnson (2015) that tCSWs can also be generated by wind-stress forcing, even when applied in the far field. Without continuous forcing these trapped modes would be eventually be destroyed by dissipation.

The presence of stratification could alter the characteristics of CSWs significantly, since the wave frequency increases at all alongshore wavenumbers (Mysak 1980; Brink 1991). For a shelf with sufficiently strong stratification, the group velocity is generally in the same direction as the phase velocity and at high wavenumbers the wave frequency increases monotonically to the inertial frequency $f$. The short waves carrying energy in the opposite direction of long waves disappear and so trapping is impossible. For sufficiently weak stratified shelves, however, some subinertial waves remain evanescent (Huthnance 1978; Chapman 1983), and as shown in Rodney & Johnson (2012) (in the rigid-lid case) trapping is possible in a reduced range of frequencies.

## Acknowledgements

This work was co-funded by the European Regional Development Fund and the Republic of Cyprus through the Research and Innovation Foundation (project: POST-DOC/0916/0138)

https://doi.org/10.1017/jfm.2020.656 Published online by Cambridge University Press

**Declaration of interests**

The authors report no conflict of interest.

## Appendix A. Numerical solution for a rectilinear shelf

Following Kaoullas & Johnson (2010*a*) we cast (3.1) into a linear eigenvalue problem for $k$ with the following transformation $Y = kZ$ to give:

$$Z'' + H'/(H)Z' + H'/(H\omega)Y + (\omega^2 - 1)/(HR^2)Y = kY, \tag{A 1}$$

$$Y = kZ, \tag{A 2}$$

subject to (3.2) and (3.3) or (3.4*a*,*b*). We discretise (A 1) on a Chebyshev grid of $N$ points following Trefethen (2000) and using the appropriate differentiation matrices we get the linear eigenvalue problem

$$\begin{pmatrix} \boldsymbol{A_1} & \boldsymbol{A_2}(\omega) \\ \boldsymbol{I} & \boldsymbol{0} \end{pmatrix} = k \begin{pmatrix} \boldsymbol{Y} \\ \boldsymbol{Z} \end{pmatrix}, \tag{A 3}$$

where $\boldsymbol{A_1}$ and $\boldsymbol{A_2}(\omega)$ are the discrete form of the left-hand side of (A 1). To impose the b.c. (3.2) at the coast $-\omega Y' = kY$ we replace the last rows of $\boldsymbol{A_1}$ and $\boldsymbol{A_2}(\omega)$ with the last row of the Chebyshev differentiation matrix times $-\omega$. It is worth noting that a similar condition applies for $Z$, that is $-\omega Z' = kZ$ which is imposed by replacing the last rows of $\boldsymbol{I}$ and $\boldsymbol{0}$ in a similar manner. Imposing this b.c. 'twice' results in a much better conditioned matrix, and also removes some spurious eigenvalues. The approximate b.c. (3.3) is imposed in exactly the same manner (the first rows are replaced now) to give an $N \times N$ linear eigenvalue problem to be solved by standard numerical packages for each set value of the frequency $\omega$.

The open ocean unapproximated b.c. (3.4*a*,*b*) is imposed by removing the first row and column of each matrix in (A 3) thus giving an $N - 2 \times N - 2$ linear eigenvalue problem.

## Appendix B. Asymptotic solution in the rigid-lid case

The leading-order equation is

$$(h\Psi^c_y)_y + h(2b\mu/\omega_0 - \mu^2)\Psi^c = 0, \tag{B 1}$$

$$\omega_0\Psi^c_y + \mu\Psi^c = 0, \quad y = 0, 1. \tag{B 2}$$

This equation is close to the stream function formulation in Kaoullas & Johnson (2012), with $h$ appearing as $h^{-1}$ and also the b.c.s (B 2) replacing Dirichlet conditions. The solution of (B 1) satisfying (B 2) is

$$\Psi^c = C\,\mathrm{e}^{-by}\,(\cos\lambda y + I\sin\lambda y)\,, \tag{B 3}$$

where

$$\lambda^2 = \frac{2b\mu}{\omega_0} - b^2 - \mu^2 = \frac{b^2}{\omega_0^2} - b^2, \quad I = \frac{b\omega_0 - \mu}{\omega_0\lambda} = -\frac{\lambda}{b}, \quad C = \sqrt{2}\omega_0\,\mathrm{e}^b, \quad \lambda = n\pi \tag{B 4$a$–$d$}$$

and

$$b = k_0\omega_0 = \mu\omega_0. \tag{B 5}$$

The first term of (B 4) is the dispersion relation for the unperturbed channel, as in the stream function formulation. Even though the two differential operators are different, their

https://doi.org/10.1017/jfm.2020.656 Published online by Cambridge University Press

spectrum is the same, as expected, since the underlying physical problem, (i.e. the rigid-lid case) is the same. At the next order:

$$(h\Psi_{1_y})_y + (2b\mu/\omega_0 - \mu^2)h\Psi_1 - (2b\mu\omega_1/\omega_0^2)h\Psi^c f_0 = 0, \tag{B 6}$$

$$\mathrm{i}\omega_0\Psi_{1_y} + \mathrm{i}\mu\Psi_1 + \mathrm{i}\omega_1 f_0\Psi_y^c + f_{0_\xi}\Psi^c = 0, \quad y = 0, 1. \tag{B 7}$$

The solvability condition becomes

$$2\omega_1(\mu^2/\omega_0)f_0 = 0, \tag{B 8}$$

which immediately forces $\omega_1 = 0$. Now $\Psi_1$ is the solution of

$$\Psi_{1_{yy}} + 2b\Psi_{1_y} + \left(2b\mu/\omega_0 - \mu^2\right)\Psi_1 = 0, \tag{B 9}$$

$$\omega_0\Psi_{1_y} + \mu\Psi_1 = \mathrm{i}f_{0_\xi}\Psi^c, \quad y = 0, 1, \tag{B 10}$$

giving

$$\Psi_1 = C\,\mathrm{e}^{-by}\,(\cos\lambda y + I\sin\lambda y)\,f_1(\xi) + (\mathrm{i}C/\omega_0\lambda)\,\mathrm{e}^{-by}\sin\lambda y f_{0_\xi}. \tag{B 11}$$

The order $\epsilon^2$ equation is

$$\begin{aligned}(h\Psi_{2_y})_y + (2b\mu/\omega_0 - \mu^2)h\Psi_2 - (2b\mu\omega_2/\omega_0^2)h\Psi^c f_0 + f_{0_{\xi\xi}}\Psi^c \\ + \alpha\gamma 2b(1-2y)(\Psi_y^c + (\mu/\omega_0)\Psi^c)f_0 = 0,\end{aligned} \tag{B 12}$$

$$\mathrm{i}\omega_0\Psi_{2_y} + \mathrm{i}\mu\Psi_2 + \mathrm{i}\omega_2 f_0\Psi_y^c + \Psi_{1_\xi} = 0, \quad y = 0, 1. \tag{B 13}$$

Multiplying (B 12) by $\Psi^c$ and integrating gives

$$I_1 f_{0_{\xi\xi}} + V(\xi)f_0 = \omega_2 I_2 f_0, \tag{B 14}$$

where

$$\begin{aligned}V(\xi) &= \alpha\gamma 2b\int_0^1 h(1-2y)(\Psi^c\Psi_y^c + (\mu/\omega_0)\Psi^{c2}) \\ &= -2b\alpha\gamma,\end{aligned} \tag{B 15}$$

$$I_1 = 1, \quad I_2 = 2\mu^2/\omega_0. \tag{B 16$a$,$b$}$$

Since the sign of the potential $V$ depends solely on $\alpha$, it can be determined from (4.34) that trapped modes exist only when $\alpha < 0$ (submerged ridge). The analysis here for a rigid-lid can be followed in terms of the stream function instead of the pressure and, as expected, leads to the same expressions (B 14), (B 15) and (B 16).

## Appendix C. Numerical solution for a non-rectilinear shelf

The waveguide in § 4 is truncated to a rectangular, discretised domain, forming a grid with $M$ points in the $x$ direction and $N$ points in the $y$ direction. Introducing the column

https://doi.org/10.1017/jfm.2020.656 Published online by Cambridge University Press

vector $\boldsymbol{p}$ as the discrete values of $\Psi$ on the rectangular domain, (4.39) can be written in its discrete form as,

$$\omega^4\boldsymbol{A}\boldsymbol{p} + \omega^2\boldsymbol{B}\boldsymbol{p} + \omega\boldsymbol{C}\boldsymbol{p} + \boldsymbol{E}\boldsymbol{p} = \boldsymbol{0}, \tag{C 1}$$

where the $MN \times MN$ matrices are given by

$$\boldsymbol{A} = 1/(\boldsymbol{H}R^2), \tag{C 2}$$

$$\boldsymbol{B} = \boldsymbol{D}_x^2 + \boldsymbol{D}_y^2 + 2b(\boldsymbol{P}_x\boldsymbol{D}_x + \boldsymbol{P}_y\boldsymbol{D}_y) - 1/(\boldsymbol{H}R^2), \tag{C 3}$$

$$\boldsymbol{C} = 2b\mathrm{i}((\boldsymbol{I} - \boldsymbol{P}_y)\boldsymbol{D}_x + \boldsymbol{P}_x(\boldsymbol{D}_y + b\boldsymbol{I})), \tag{C 4}$$

$$\boldsymbol{E} = b^2(2\boldsymbol{P}_y - \boldsymbol{I}), \tag{C 5}$$

the matrices $\boldsymbol{D}_y^2$ are $\boldsymbol{H}$, and $\boldsymbol{P}_x$, $\boldsymbol{P}_y$ are the discrete values of the topography function (4.8) and (4.10*a*,*b*). Finally, the differentiation matrices $\boldsymbol{D}_y^i$ and $\boldsymbol{D}_x^i$ for $i = 1, 2$ are the appropriate tensor products with the identity matrix, of the Chebyshev differentiation matrix and the Laguerre differentiation matrix, respectively, as defined in Weideman & Reddy (2000).

Accuracy can be greatly improved by shifting the frequency $\omega$ to the cutoff frequency of the rectilinear shelf $\omega_0$ with $\omega = \omega_0 + \lambda$ to give from (C 1),

$$\lambda^4\boldsymbol{A_1}\boldsymbol{p} + \lambda^3\boldsymbol{A}_2\boldsymbol{p} + \lambda^2\boldsymbol{A_3}\boldsymbol{p} + \lambda\boldsymbol{A_4}\boldsymbol{p} + \boldsymbol{A_5}\boldsymbol{p} = \boldsymbol{0}, \tag{C 6}$$

where,

$$\boldsymbol{A_1} = \boldsymbol{A}, \tag{C 7}$$

$$\boldsymbol{A_2} = 4\omega_0\boldsymbol{A}, \tag{C 8}$$

$$\boldsymbol{A_3} = 6\omega_0^2\boldsymbol{A} + \boldsymbol{B}, \tag{C 9}$$

$$\boldsymbol{A_4} = 4\omega_0^3\boldsymbol{A} + 2\omega_0\boldsymbol{B} + \boldsymbol{C}, \tag{C 10}$$

$$\boldsymbol{A_5} = \omega_0^4\boldsymbol{A} + \omega_0^2\boldsymbol{B} + \omega_0\boldsymbol{C} + \boldsymbol{E}. \tag{C 11}$$

The b.c.s (4.40) now become

$$\lambda^2\boldsymbol{D}_y\boldsymbol{p} + \lambda(2\omega_0\boldsymbol{D}_y - \mathrm{i}\boldsymbol{D}_x)\boldsymbol{p} + (\omega_0^2\boldsymbol{D}_y - 2\omega_0\mathrm{i}\boldsymbol{D}_x + b\boldsymbol{I})\boldsymbol{p} = \boldsymbol{0}, \quad y = 0, 1, \tag{C 12}$$

and will be imposed on (C 6) by replacing the appropriate rows of matrices (C 7)–(C 11) for the corresponding power of $\lambda$. Let us consider the $\lambda^4$ case, which has the $\boldsymbol{0}$ matrix as a coefficient in (C 12). Here, to impose the b.c. at $y = 1$ we need to replace the $1 + (n - 1)N$, $(n = 1, \ldots, M)$ rows of matrix $\boldsymbol{A_1}$ with the corresponding rows of the $\boldsymbol{0}$ matrix, and to impose the b.c. at $y = 0$ we need to replace the $nN$, $(n = 1, \ldots, M)$ rows of these matrices. In a similar manner we can impose the b.c.s to the other matrix coefficients of (C 6). Finally, to linearise the fourth-order polynomial eigenvalue problem (4.40) to a generalised eigenvalue problem we introduce the following linearisation:

$$\boldsymbol{q} = \lambda\boldsymbol{p}, \quad \boldsymbol{r} = \lambda\boldsymbol{q}, \quad \boldsymbol{s} = \lambda\boldsymbol{r}, \tag{C 13$a$–$c$}$$

to give

$$\begin{pmatrix} \boldsymbol{A_5} & \boldsymbol{A_4} & \boldsymbol{A_3} & \boldsymbol{A}_2 \\ \boldsymbol{0} & \boldsymbol{I} & \boldsymbol{0} & \boldsymbol{0} \\ \boldsymbol{0} & \boldsymbol{0} & \boldsymbol{I} & \boldsymbol{0} \\ \boldsymbol{0} & \boldsymbol{0} & \boldsymbol{0} & \boldsymbol{I} \end{pmatrix} \begin{pmatrix} \boldsymbol{p} \\ \boldsymbol{q} \\ \boldsymbol{r} \\ \boldsymbol{s} \end{pmatrix} = \lambda \begin{pmatrix} -\boldsymbol{A_1} & \boldsymbol{0} & \boldsymbol{0} & \boldsymbol{0} \\ \boldsymbol{I} & \boldsymbol{0} & \boldsymbol{0} & \boldsymbol{0} \\ \boldsymbol{0} & \boldsymbol{I} & \boldsymbol{0} & \boldsymbol{0} \\ \boldsymbol{0} & \boldsymbol{0} & \boldsymbol{I} & \boldsymbol{0} \end{pmatrix} \begin{pmatrix} \boldsymbol{p} \\ \boldsymbol{q} \\ \boldsymbol{r} \\ \boldsymbol{s} \end{pmatrix}. \tag{C 14}$$

https://doi.org/10.1017/jfm.2020.656 Published online by Cambridge University Press

Even though it is a $4MN \times 4MN$ generalised eigenvalue problem, the matrices are very sparse and thus can be solved with any sparse eigenvalue finder routine.

## REFERENCES


ADAMS, J. K. & BUCHWALD, V. T. 1969 The generation of continental shelf waves. *J. Fluid Mech.* **35** (4), 815–826.

ADVANPIX 2019 Multiprecision Computing Toolbox for MATLAB. Available at: www.advanpix.com.

ASLANYAN, A., PARNOVSKI, L. & VASSILIEV, D. 2000 Complex resonances in acoustic waveguides. *Q. J. Mech. Appl. Maths* **53** (3), 429–447.

BRINK, K. H. 1991 Coastal-trapped waves and wind-driven currents over the continental shelf. *Annu. Rev. Fluid Mech.* **23** (1), 389–412.

BUCHWALD, V. T. & ADAMS, J. K. 1968 The propagation of continental shelf waves. *Proc. R. Soc. Lond.* A **305** (1481), 235–250.

CHAPMAN, D. C. 1983 On the influence of stratification and continental shelf and slope topography on the dispersion of subinertial coastally trapped waves. *J. Phys. Oceanogr.* **13** (9), 1641–1652.

DAVIES, E. B. & PARNOVSKI, L. 1998 Trapped modes in acoustic waveguides. *Q. J. Mech. Appl. Maths* **51** (3), 477–492.

DITTRICH, J. & KRIZ, J. 2002 Curved planar quantum wires with Dirichlet and Neumann boundary conditions. *J. Phys.* A **35** (20), L269–L275.

DUCLOS, P. & EXNER, P. 1995 Curvature-induced bound states in quantum waveguides in two and three dimensions. *Rev. Math. Phys.* **7**, 73–102.

EVANS, D. V., LEVITIN, M. & VASSILIEV, D. 1994 Existence theorems for trapped modes. *J. Fluid Mech.* **261**, 21–31.

EXNER, P. & SEBA, P. 1989 Bound states in curved quantum waveguides. *J. Math. Phys.* **30** (11), 2574–2580.

GRIDIN, D., CRASTER, R. V. & ADAMOU, A. T. I. 2005 Trapped modes in curved elastic plates. *Proc. R. Soc. Lond.* A **461** (2064), 1181–1197.

GRIMSHAW, R. 1977 The effects of a variable coriolis parameter, coastline curvature and variable bottom topography on continental shelf waves. *J. Phys. Oceanogr.* **7** (4), 547–554.

HUTHNANCE, J. M. 1975 On trapped waves over a continental shelf. *J. Fluid Mech.* **69** (4), 689–704.

HUTHNANCE, J. M. 1978 Coastal trapped waves - analysis and numerical-calculation by inverse iteration. *J. Phys. Oceanogr.* **8** (1), 74–92.

HUTHNANCE, J. M. 1987 Effects of longshore shelf variations on barotropic continental shelf waves, slope currents and ocean modes. *Prog. Oceanogr.* **19** (2), 177–220.

JOHNSON, E. R. 1989 Topographic waves in open domains. Part 1. Boundary conditions and frequency estimates. *J. Fluid Mech.* **200**, 69–76.

JOHNSON, E. R. & KAOULLAS, G. 2011 Bay-trapped low-frequency oscillations in lakes. *Geophys. Astrophys. Fluid Dyn.* **105** (1), 48–60.

JOHNSON, E. R., LEVITIN, M. & PARNOVSKI, L. 2006 Existence of eigenvalues of a linear operator pencil in a curved waveguide—localized shelf waves on a curved coast. *SIAM J. Math. Anal.* **37** (5), 1465–1481.

KAOULLAS, G. & JOHNSON, E. R. 2010*a* Fast accurate computation of shelf waves for arbitrary depth profiles. *Cont. Shelf Res.* **30** (7), 833–836.

KAOULLAS, G. & JOHNSON, E. R. 2010*b* Geographically localised shelf waves on curved coasts. *Cont. Shelf Res.* **30** (15), 1753–1760.

KAOULLAS, G. & JOHNSON, E. R. 2012 Isobath variation and trapping of continental shelf waves. *J. Fluid Mech.* **700**, 283–303.

KAPLUNOV, J. D., ROGERSON, G. A. & TOVSTIK, P. E. 2005 Localized vibration in elastic structures with slowly varying thickness. *Q. J. Mech. Appl. Maths* **58** (4), 645–664.

KREJČIŘÍK, D. & KŘÍŽ, J. 2005 On the spectrum of curved planar waveguides. *Publ. Res. Inst. Math. Sci.* **41** (3), 757–791.

LANDAU, L. D. & LIFSHITZ, E. M. 1991 *Quantum Mechanics Non-Relativistic Theory*, vol. 3. Butterworth-Heinemann.


https://doi.org/10.1017/jfm.2020.656 Published online by Cambridge University Press

LeBlond, P. H. & Mysak, L. A. 1978 *Waves in the Ocean*. Elsevier.

Linton, C. & McIver, M. 1998 Trapped modes in cylindrical waveguides. *Q. J. Mech. Appl. Maths* **51**, 389–412.

Linton, C. M. & McIver, P. 2007 Embedded trapped modes in water waves and acoustics. *Wave Motion* **45** (1), 16–29.

Mysak, L. A. 1980 Recent advances in shelf wave dynamics. *Rev. Geophys. Space Phys.* **18** (1), 211–241.

Postnova, J. & Craster, R. V. 2008 Trapped modes in elastic plates, ocean and quantum waveguides. *Wave Motion* **45** (4), 565–579.

Proudman, J. 1929 On a general expansion in the theory of the tides. *Proc. Lond. Math. Soc.* **s2-29** (1), 527–536.

Rhines, P. 1969 Slow oscillations in an ocean of varying depth. Part 1. Abrupt topography. *J. Fluid Mech.* **37**, 161–189.

Robinson, A. R. 1964 Continental shelf waves and the response to of sea level to weather systems. *J. Geophys. Res.* **69** (2), 367–368.

Rocha, C. B., Bossy, T., Llewellyn Smith, S. G. & Young, W. R. 2020 Improved bounds on horizontal convection. *J. Fluid Mech.* **883**, A41.

Rodney, J. T. & Johnson, E. R. 2012 Localisation of coastal trapped waves by longshore variations in bottom topography. *Cont. Shelf Res.* **32**, 130–137.

Rodney, J. T. & Johnson, E. R. 2015 Localised continental shelf waves: geometric effects and resonant forcing. *J. Fluid Mech.* **785**, 54–77.

Schulz, William J., Mied, Richard P. & Snow, Charlotte M. 2012 Continental shelf wave propagation in the mid-atlantic bight: a general dispersion relation. *J. Phys. Oceanogr.* **42** (4), 558–568.

Shen, J. & Wang, L.-L. 2009 Some recent advances on spectral methods for unbounded domains. *Commun. Comput. Phys.* **5** (2–4), 195–241.

Tang, T. 1993 The Hermite spectral method for Gaussian-type functions. *SIAM J. Sci. Comput.* **14** (3), 594–606.

Tisseur, F. 2000 Backward error and condition of polynomial eigenvalue problems. *Linear Algebr. Applics.* **309** (1), 339–361.

Trefethen, L. N. 2000 *Spectral Methods in MATLAB*. SIAM.

Weideman, J. A. C. & Reddy, S. C. 2000 A MATLAB differentiation matrix suite. *ACM Trans. Math. Softw.* **26** (4), 465–519.

https://doi.org/10.1017/jfm.2020.656 Published online by Cambridge University Press